Low-Frequency Velocity Correlation Spectrum of Fluid in a Rectangular Microcapillary

José A. Fornés* and José M. Ortiz de Zárate

Departamento de Física Aplicada I, Facultad de Ciencias Físicas, Universidad Complutense, E-28040 Madrid, Spain

Received August 13, 2007

In addition to the fast correlation for local stochastic motion, the velocity correlation function in a fluid enclosed within the pore boundaries features a slow long time-tail decay. At late times, the flow approaches that of an incompressible fluid. Here, we consider the motion of a viscous fluid, at constant temperature, in a rectangular semipermeable channel. The fluid is driven through the rectangular capillary by a uniform main pressure gradient. Tiny pressure gradients are allowed perpendicular to the main flux. We solve numerically the three-dimensional Navier−Stokes equations for the velocity field to obtain the steady solution. We then set and solve the Langevin equation for the fluid velocity. We report hydrodynamic fluctuations for the center-line velocity together with the corresponding relaxation times as a function of the size of the observing region and the Reynolds number. The effective diffusion coefficient for the fluid in the microchannel is also estimated ($D_{\text{eff}} = 1.43 \times 10^{-10}$ m^2·s^{-1} for $Re = 2$), which is in accordance with measurements reported for a similar system (Stepišnik, J.; Callaghan, P. T. *Physica B* **2000**, *292*, 296−301; Stepišnik, J.; Callaghan, P. T. *Magn. Reson. Imaging* **2001**, *19*, 469-472).

I. Introduction

In recent years, with the advance of nanotechnology, there has been interest in the fabrication of nanoscale devices powered by[1] or constructed using[2] so-called "Brownian motors". Also, a series of pressure-sensitive microfluidic gates to regulate liquid flow have been successfully fabricated.[3] Yang and Kwok studied the microfluid flow with hydrophobic channel walls with electrokinetic effects and Navier's slip condition.[4] Optical detection of a single molecule in solution has become more and more important.[5−7] Lenne et al.[8] and also Gösch et al.[9] reported hydrodynamic and electrophoretic flow profiling in microchannel structures by single molecule fluorescence correlation spectroscopy (FCS), where the flow measured showed a Poiseuille laminar flow profile. Computer simulations of fluid hydrodynamics by Alder and Wainwright[10] and Hagen et al.[11] revealed the existence of slow molecular motion, that appears as a long time tail of the velocity correlation function superposed on the fast exponential decay of the propagating sound mode, which does not contribute to the long time tail. At late times, the flow approaches that of an incompressible fluid. This results were proved experimentally by Stepišnik and Callaghan[12,13] who applied the NMR modulated gradient spin−echo method (MGSE)[14] to measure the diffusion coefficient. In this work, we shall report the influence of hydrodynamic fluctuations on the mean center-line velocity of an incompressible fluid in a rectangular cross section microcapillary channel. With such an aim, we set and solve the coupled Langevin equations for the three components of the fluid velocity. We also report the relaxation time of the hydrodynamic fluctuations as a function of the volume and Reynolds number. In this first approximation to the problem, we consider the temperature uniform and constant through the whole cell. As a consequence, we neglect the hydrodynamic heat equation (energy balance) in our development. This is justified, and as an example we can consider that the heating effects in fluorescence correlation spectroscopy (FCS) are negligible at the laser intensities used. The steady-state difference, ΔT, between the temperature of the solution at the center of the Gaussian beam and the ambient temperature is $\Delta T \leq 10^{-6}$ K.[15]

II. Hydrodynamic Fluctuations

The hydrodynamic equations relevant to our problem (see ref 16) are as follows:

$$\frac{\partial \rho}{\partial t} + \nabla(\rho \mathbf{v}) = 0 \tag{1}$$

$$\rho \frac{\partial v_i}{\partial t} + \rho v_k \frac{\partial v_i}{\partial x_k} = -\frac{\partial p}{\partial x_i} + \frac{\partial \sigma'_{ik}}{\partial x_k} \tag{2}$$

where $v(x,y,z,t)$, $p(x,y,z,t)$, and $\rho(x,y,z,t)$ are the velocity (m/s), the pressure (N/m), and the mass density (kg/m^3) of the fluid, respectively. The symbol v_i represents the components of the velocity in the corresponding coordinates system. The dissipative fluxes are the heat flow $\mathbf{q}$ (W/m^2) and the deviatoric stress tensor σ'_{ik} (N/m^2), to be distinguished from the stress tensor σ_{ik}

* To whom correspondence should be addressed. E-mail: jafornes@fis.ucm.es.

(1) Soong, R. K.; Bachand, G. D.; Neves, H. P.; Olkhovets, A. G.; Craihead, H. G.; Montemagno, C. D. *Science* **2000**, *290*, 1555.
(2) Tsong, T. Y. *J. Biol. Phys.* **2002**, *28*, 309−325.
(3) Zhao, B.; Moore, J. S.; Beebe, D. J. *Langmuir* **2003**, *19* (5), 1873−1879.
(4) Yang, J.; Kwok, D. Y. *Langmuir* **2003**, *19* (4), 1047−1053.
(5) Eigen, M.; Rigler, R. *Proc. Natl. Acad. Sci. U.S.A.* **1994**, *91*, 5740−5747.
(6) Goodwin, P. M.; Johnson, M. E.; Martin, J. C.; Ambrose, W. P.; Marrone, B. L.; Jett, J. H.; Keller, R. A. *Nucleic Acids Res.* **1993**, *21*, 803−806.
(7) Sauer, M.; Angerer, B.; Ankenbauer, W.; Foldes-Papp, Z.; Gobel, F.; Han, K. T.; Rigler, R.; Schulz, A.; Wolfrum, J.; Zander, C. J. *J. Biotechnol.* **2001**, *85*, 181−201.
(8) Lenne, P. F.; Colombo, D.; Giovannini, H.; Rigneault, H. *Single Mol.* **2002**, *3* (4), 194−200.
(9) Gösch, M.; Blom, H.; Holm, J.; Heino, T.; Rigler, R. *Anal. Chem.* **2000**, *72* (14), 3260−3265.
(10) Alder, B. J.; Wainwright, T. E. *Phys. Rev. A* **1970**, *1*, 18−21.
(11) Hagen, M. H. J.; Pagonabarraga, I.; Lowe, C. P.; Frenkel, D. *Phys. Rev Lett.* **1997**, *78* (19), 3785−3788.
(12) Stepišnik, J.; Callaghan, P. T. *Physica B* **2000**, *292*, 296−301.
(13) Stepišnik, J.; Callaghan, P. T. *Magn. Reson. Imaging* **2001**, *19*, 469−472.
(14) Callaghan, P. T.; Stepišnik, J. *J. Magn. Res. A* **1995**, *117*, 118−122.
(15) Magde, D.; Edson, E. L.; Webb, W. W. *Biopolymers* **1974**, *13* (1), 29−61.
(16) Lifshitz, E. M.; Pitaevskii, L. P. *Statistical Physics*; Course of Theoretical Physics, Vol. 9, Part 2; Butterworth-Heinemann: Oxford, 2003.

10.1021/la702502q CCC: $37.00
Published on Web 10/16/2007

$$\sigma_{ik} = -p\delta_{ik} + \sigma'_{ik} \tag{3}$$

Hydrodynamic equations need to be supplemented with boundary conditions. Molecular forces always exist between a viscous fluid and a solid surface. These forces cause the fluid layer just at the surface to be at rest and as a consequence have to be considered as a boundary condition of the movement equations. The velocity of the fluid is zero at the solid surfaces, and this is the so-called no-slip boundary condition ($v = 0$). This is not our case of semipermeable walls to abandon the no-slip boundary condition. For a recent review with a deep discussion on the no-slip boundary condition, including microfluidics, see Lauga et al.[17] and references therein. In any case, since we are interested in bulk fluctuations here and our channel size is in the micrometer range, the choice of boundary conditions would not affect our results.

The (deviatoric) stress tensor and the heat flow are related to the velocity by the Newton viscosity law and the Fourier law, respectively. However, when fluctuations are present, there also appear local stresses and spontaneous energy fluxes disconnected from those gradients. The "random" contributions to the dissipative fluxes will be designed by s_{ik} and $\mathbf{g}$. The fluctuating phenomenological laws then read as

$$\sigma'_{ik} = \eta\left(\frac{\partial v_i}{\partial x_k} + \frac{\partial v_k}{\partial x_i} - \frac{2}{3}\delta_{ik}\,\nabla\cdot\mathbf{v}\right) + \zeta\,\delta_{ik}\,\nabla\cdot\mathbf{v} + s_{ik} \tag{4}$$

$$\mathbf{q} = -\kappa\nabla T + \mathbf{g} \tag{5}$$

The term inside the brackets in eq 4 cancels for $i = k$. The constants η and ζ are called viscocity coefficients ($N\cdot s\cdot m^{-2}$) where both are positives, and κ ($W\cdot m^{-1}\cdot K^{-1}$) is the thermal conductivity. As a consequence of eq 4, the quantity $\partial\sigma'_{ik}/\partial x_k$ in the momentum balance (eq 2) can be written as

$$\frac{\partial\sigma'_{ik}}{\partial x_k} = \eta\Delta\mathbf{v} + \left(\zeta + \frac{1}{3}\eta\right)\nabla(\nabla\cdot\mathbf{v}) + \frac{\partial s_{ik}}{\partial x_k} \tag{6}$$

so that eq 2, for a viscous fluid in movement, can be expressed as a single vectorial equation:

$$\rho\left[\frac{\partial\mathbf{v}}{\partial t} + (\mathbf{v}\cdot\nabla)\mathbf{v}\right] = -\nabla p + \eta\Delta\mathbf{v} + \left(\zeta + \frac{1}{3}\eta\right)\nabla(\nabla\cdot\mathbf{v}) + \frac{\partial s_{ik}}{\partial x_k} \tag{7}$$

When the fluid can be considered as incompressible, then $\nabla\cdot\mathbf{v} = 0$. As a consequence, the equation of movement of an incompressible viscous fluid is simply given by

$$\frac{\partial\mathbf{v}}{\partial t} = -(\mathbf{v}\cdot\nabla)\mathbf{v} - \frac{1}{\rho}\nabla p + \frac{\eta}{\rho}\nabla^2\mathbf{v} + \frac{1}{\rho}\frac{\partial s_{ik}}{\partial x_k} \tag{8}$$

This equation, without the last term, is the Navier−Stokes equation. The first term in the right-hand side expresses convection, the second term represents pressure variations, the third term represents the viscous forces, and the fourth one represents fluctuations. We observe that, for an incompressible fluid, only one viscosity coefficient appears in the equation of motion. As most of the fluids can be considered as (nearly) incompressible, the shear viscosity coefficient η is the only relevant one in practice. The ratio

$$\nu = \frac{\eta}{\rho} \tag{9}$$

is referred to as kinematic viscocity ($J\cdot s\cdot kg^{-1}$) (while η itself is referred to as the dynamic shear viscocity).

The energy dissipated in an incompressible fluid due to viscous processes can be written (see ref 16) as

$$E_{\mathrm{diss}} = -\frac{1}{2}\eta\int\left(\frac{\partial v_i}{\partial x_k} + \frac{\partial v_k}{\partial x_i}\right)^2 \mathrm{d}V \tag{10}$$

As already mentioned above, in this paper, we shall consider a perfectly isothermal system, and this approximation neglects the heating effects expressed by eq 10.

A. Discretization of the Langevin Equation for the Velocity. To numerically solve eq 8, we need to perform a discretization. This is achieved by multiplying both members by dt and performing the integration in the interval (t,$t + \Delta t$), namely

$$\Delta\mathbf{v} = -\int_t^{t+\Delta t}(\mathbf{v}\cdot\nabla)\mathbf{v}\,\mathrm{d}t - \frac{1}{\rho}\int_t^{t+\Delta t}\nabla p\,\mathrm{d}t + \nu\int_t^{t+\Delta t}\nabla^2\mathbf{v}\,\mathrm{d}t + \frac{1}{\rho}\int_t^{t+\Delta t}\frac{\partial s_{ik}}{\partial x_k}\mathrm{d}t \tag{11}$$

or

$$\Delta\mathbf{v} = -\overline{(\mathbf{v}\cdot\nabla)\mathbf{v}}\Delta t - \frac{1}{\rho}\overline{\nabla p}\Delta t + \nu\overline{\nabla^2\mathbf{v}}\Delta t + \frac{C_i}{\rho}\Delta W(t) \tag{12}$$

where the discretization of the stochastic forcing term has been performed by employing eq 48 of the Appendix, where the coefficients C_i and the "Wiener's increment" $\Delta W(t)$ are defined and the discretization of the random force is justified in more detail.

At the limit $\Delta t \to \mathrm{d}t$, the mean values $\overline{(\mathbf{v}\cdot\nabla)\mathbf{v}} \simeq (\mathbf{v}\cdot\nabla)\mathbf{v}$, $\overline{\nabla p} \simeq \nabla p$, and $\overline{\nabla^2\mathbf{v}} \simeq \nabla^2\mathbf{v}$, while $\Delta W(t) = \mathrm{d}W(t)$. From the developments in the Appendix, we need to recall here that the "Wiener's process" d$W(t)$ is just a Gaussian stochastic process of width $\sigma = (\mathrm{d}t)^{1/2}$. At each pass of the integration, we then have to draw d$W(t)$ and normalize the result properly. That is to say, if R_G is an aleatory number, with a Gaussian distribution, centered in $R_G = 0$ and width 1, then we can write at each integration step $\mathrm{d}W(t) = (\mathrm{d}t)^{1/2}R_G$. To conclude the discretization process, eq 12 is transformed in the corresponding Euler's equation, giving the temporal evolution of the velocity, namely

$$\mathbf{v}^{n+1} = \mathbf{v}^n - (\mathbf{v}^n\cdot\nabla)\mathbf{v}^n\,\mathrm{d}t - \frac{1}{\rho}\nabla p\,\mathrm{d}t + \nu\nabla^2\mathbf{v}^n\,\mathrm{d}t + \frac{C_i}{\rho}\mathrm{d}t^{1/2}\,R_G \tag{13}$$

The relaxation time τ_σ of the hydrodynamic fluctuations is then

$$\tau_\sigma = \left(\frac{U_{CL}\rho}{C_i}\right)^2 \tag{14}$$

where U_{CL} is the center-line velocity (see below). From now on, the averages $\langle ...\rangle$ are over the realizations of the stochastic process.

In this paper, we shall be concerned with the evaluation of several statistical parameters. A first basic quantity will be the variance of the velocity, namely

$$\sigma_{\mathbf{v}}{}^2 = \langle\mathbf{v}(t)^2\rangle - \langle\mathbf{v}(t)\rangle^2 \tag{15}$$

(17) Lauga, E.; Brenner, M. P.; Stone, H. A. *Handbook of Experimental Fluid Dynamics*; Foss, J., Tropea, C., Yarin, A., Eds.; Springer-Verlag: New York, 2005.

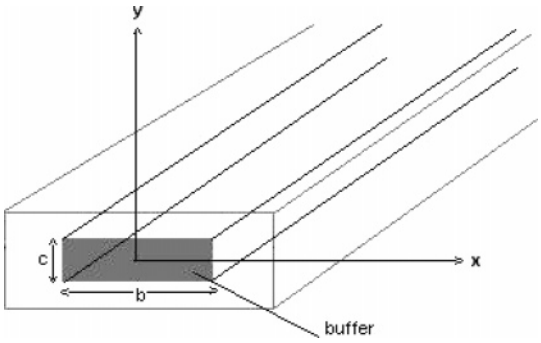

Figure 1. Schematic drawing of the channel.

Another quantity of central interest is the average position, namely

$$\langle \mathbf{r}(t) \rangle = \langle \int_0^t \mathbf{v}(t)\, \mathrm{d}t \rangle \tag{16}$$

The corresponding variance of the position is

$$\sigma_{\mathbf{r}}{}^2 = \langle \mathbf{r}(t)^2 \rangle - \langle \mathbf{r}(t) \rangle^2 \tag{17}$$

Associated to $\sigma_{\mathbf{r}}$, an effective diffusion coefficient can be defined as the long time limit (i.e., after transients due to initial conditions have died out):

$$D_{\mathrm{eff}} = \lim_{t\to\infty} \frac{\sigma_{\mathbf{r}}{}^2}{2t} \tag{18}$$

B. Equations for a Rectangular Cross Section Pipe. *1. The System.* We consider an incompressible viscous fluid of kinematic viscosity ν and uniform density ρ driven in a rectangular pipe with rectangular cross section with the size along the x axis (width b) being much larger than the size along the y axis (height c). The length of the pipe is denoted by L. A schematic drawing of the channel is shown in Figure 1. The flow is driven by a uniform pressure gradient, $\partial_z p = K$, along the pipe and parallel to the z axis. The system is subjected to thermal noise at the constant temperature T. Furthermore, we assume tiny pressure gradients perpendicular to the z direction with $\partial_x p = \partial_y p = 10^{-2}\partial_z p$, causing small axial fluid fluxes. In this sense, we can consider our system as a semipermeable pipe. The existence of these lateral fluxes allows the coupling of the three components of the velocity field, and the nonexistence of them renders only one equation. Also, these fluxes are common in experimental systems as in pervaporation in channels; see, for instance, ref 18.

2. The Equations. To simplify the working equations, all variables will be rendered dimensionless using d_{h} and the centerline velocity U_{CL} (both defined below). Hence, time will be measured in units of $d_{\mathrm{h}}U_{\mathrm{CL}}{}^{-1}$, pressure will be measured in units of $\rho U_{\mathrm{CL}}{}^2$, the pressure gradient will be measured in units of $\rho U_{\mathrm{CL}}{}^2 d_{\mathrm{h}}{}^{-1}$, energy will be measured in units of $\rho U_{\mathrm{CL}}{}^2 d_{\mathrm{h}}{}^3$, and forces will be measured in units of $\rho U_{\mathrm{CL}}{}^2 d_{\mathrm{h}}{}^2$. In addition, the viscosity η will be measured in units of $\rho U_{\mathrm{CL}} d_{\mathrm{h}}$ and the random force $\partial_{xk} s_{ik}$ will be measured in units of $\rho U_{\mathrm{CL}}{}^2 d_{\mathrm{h}}{}^{-1}$.

The Reynolds number is the parameter governing the dynamics of the system and is defined by

$$Re = \frac{d_{\mathrm{h}} U_{\mathrm{CL}}}{\nu} \tag{19}$$

and d_{h} is the hydraulic diameter, which for a rectangular cross section pipe is

$$d_{\mathrm{h}} = \frac{2bc}{b+c} \tag{20}$$

After having introduced all the previous quantities, we write the dimensionless version of eq 8 as

$$\frac{\partial \mathbf{v}'}{\partial t'} = -(\mathbf{v}'\cdot\nabla)\mathbf{v}' - \nabla p' + \frac{1}{Re}\nabla^2 \mathbf{v}' + \frac{\partial s'_{ik}}{\partial x'_k} \tag{21}$$

or, if we split eq 21 in the three scalar equations corresponding to each component (x,y,z) of the velocity (u,v,w), we have

$$\partial_{t'}u' = -u'\partial_{x'}u' - v'\partial_{y'}u' - w'\partial_{z'}u' - \partial_{x'}p' + Re^{-1}\nabla^2 u' + \xi(t')C'_u \tag{22}$$

$$\partial_{t'}v' = -u'\partial_{x'}v' - v'\partial_{y'}v' - w'\partial_{z'}v' - \partial_{y'}p' + Re^{-1}\nabla^2 v' + \xi(t')C'_v \tag{23}$$

$$\partial_{t'}w' = -u'\partial_{x'}w' - v'\partial_{y'}w' - w'\partial_{z'}w' - \partial_{z'}p' + Re^{-1}\nabla^2 w' + \xi(t')C'_w \tag{24}$$

At the steady state, $\partial_{x'}u' = \partial_{y'}v' = \partial_{z'}w' = 0$.

To perform the numerical calculation, eq 21 can be written as

$$\mathbf{v}'^{n+1} = \mathbf{v}'^{n} - (\mathbf{v}'^{n}\cdot\nabla)\mathbf{v}'^{n}\,\mathrm{d}t' - \nabla p'\,\mathrm{d}t' + Re^{-1}\nabla^2\mathbf{v}'^{n}\,\mathrm{d}t' + C'_i(\mathrm{d}t')^{1/2}R_{\mathrm{G}} \tag{25}$$

Correspondingly, eq 14 can be written as

$$\tau_\sigma = \left(\frac{Re\eta}{d_{\mathrm{h}}C}\right)^2 = \left(\frac{Kd_{\mathrm{h}}{}^2\rho}{48\eta C}\right)^2 \tag{26}$$

where we have used eqs 14, 19, and 52. We shall also need the dimensionless constant C', which reads as

$$C' = \frac{Cd_{\mathrm{h}}{}^2}{\rho(\nu Re)^{3/2}} = \frac{-2^{1/2}(3^{-1/2}+1)(k_{\mathrm{B}}T\eta)^{1/2}(\Delta V)^{-5/6}\,d_{\mathrm{h}}{}^2}{\rho(\nu Re)^{3/2}} \tag{27}$$

with τ'_σ, the dimensionless relaxation time, related to C' by

$$\tau'_\sigma = C'^{-2} \tag{28}$$

III. Numerical Methods

Since all variables have been rendered dimensionless in the previous section, from here on we shall omit the primes in all the symbols. We start our numerical calculation by the corresponding discretization of eq 25, which proceeds in various steps. First, we write the vector $(\mathbf{v}^n\cdot\nabla)\mathbf{v}^n\,\mathrm{d}t$ in its components as

$$(\mathbf{v}^n\cdot\nabla)\mathbf{v}^n\,\mathrm{d}t \equiv \begin{pmatrix} u\partial_x u + v\partial_y u + w\partial_z u \\ u\partial_x v + v\partial_y v + w\partial_z v \\ u\partial_x w + v\partial_y w + w\partial_z w \end{pmatrix}\mathrm{d}t \tag{29}$$

Next, the first component of eq 29 is discretized as

$$\frac{1}{2}\frac{\mathrm{d}t}{\mathrm{d}x}\begin{pmatrix} u^n_{i,j,k}(u^n_{i+1,j,k} - u^n_{i-1,j,k}) + \\ v_{i,j,k}(u^n_{i,j+1,k} - u^n_{i,j-1,k}) + \\ w^n_{i,j,k}(u^n_{i,j,k+1} - u^n_{i,j,k-1}) \end{pmatrix} \tag{30}$$

and analogously, for the other components. The vector $1/Re\nabla^2\mathbf{v}^n\,\mathrm{d}t$ is treated in a similar fashion. First, it is split in its components as

(18) Villaluenga, J. P. G.; Cohen, Y. *J. Membr. Sci.* **2005**, *260*, 119−130.

$$\frac{1}{Re}\nabla^2\mathbf{v}^n\,\mathrm{d}t \equiv \frac{\mathrm{d}t}{Re}\begin{pmatrix}\nabla^2 u^n\\ \nabla^2 v^n\\ \nabla^2 w^n\end{pmatrix} \tag{31}$$

the first component is discretizated as

$$\frac{1}{Re}\frac{\mathrm{d}t}{\mathrm{d}x^2}(u^n_{i-1,j,k} + u^n_{i+1,j,k} + u^n_{i,j-1,k} + u^n_{i,j+1,k} + u^n_{i,j,k-1} + u^n_{i,j,k+1} - 6u^n_{i,j,k}) \tag{32}$$

and analogously, for the other components.

We have considered equal increments in the three coordinates, $\mathrm{d}x = \mathrm{d}y = \mathrm{d}z$, of our rectangular grid. Consequently, we have to comply with the numerical stability condition, known as CFL (Courant−Friedrichs−Lewy), which reads for our case as

$$\frac{3}{Re}\frac{\mathrm{d}t}{\mathrm{d}x^2} \le \frac{1}{2} \tag{33}$$

Taking the equal sign (most favorable case), we obtain for the ratio of time to spatial increments

$$\frac{\mathrm{d}t}{\mathrm{d}x} = \sqrt{\frac{Re\,\mathrm{d}t}{6}} \tag{34}$$

To perform the simulation surrounding the steady state, we solved simultaneously the system of the three coupled Langevin equations:

$$u^{n+1}_{i,j,k} = u^n_{i,j,k} - \sqrt{\frac{Re\,\mathrm{d}t}{24}}[v^n_{i,j,k}(u^n_{i,j+1,k} - u^n_{i,j-1,k}) + w^n_{i,j,k}(u^n_{i,j,k+1} - u^n_{i,j,k-1})] - \Pi_{0x}\,\mathrm{d}t + \frac{1}{6}(u^n_{i-1,j,k} + u^n_{i+1,j,k} + u^n_{i,j-1,k} + u^n_{i,j+1,k} + u^n_{i,j,k-1} + u^n_{i,j,k+1} - 6u^n_{i,j,k}) + C'_a\sqrt{T}\,\mathrm{d}t^{1/2}R_G$$

$$v^{n+1}_{i,j,k} = v^n_{i,j,k} - \sqrt{\frac{Re\,\mathrm{d}t}{24}}[u^n_{i,j,k}(v^n_{i+1,j,k} - v^n_{i-1,j,k}) + w^n_{i,j,k}(v^n_{i,j,k+1} - v^n_{i,j,k-1})] - \Pi_{0y}\,\mathrm{d}t + \frac{1}{6}(v^n_{i-1,j,k} + v^n_{i+1,j,k} + v^n_{i,j-1,k} + v^n_{i,j+1,k} + v^n_{i,j,k-1} + v^n_{i,j,k+1} - 6v^n_{i,j,k}) + C'_a\sqrt{T}\,\mathrm{d}t^{1/2}R_G \tag{35}$$

$$w^{n+1}_{i,j,k} = w^n_{i,j,k} - \sqrt{\frac{Re\,\mathrm{d}t}{24}}[u^n_{i,j,k}(w^n_{i+1,j,k} - w^n_{i-1,j,k}) + v^n_{i,j,k}(w^n_{i,j+1,k} - w^n_{i,j-1,k})] - \Pi_{0z}\,\mathrm{d}t + \frac{1}{6}(w^n_{i-1,j,k} + w^n_{i+1,j,k} + w^n_{i,j-1,k} + w^n_{i,j+1,k} + w^n_{i,j,k-1} + w^n_{i,j,k+1} - 6w^n_{i,j,k}) + C'_a\sqrt{T}\,\mathrm{d}t^{1/2}R_G$$

with

$$C'_a = \frac{-2^{1/2}(3^{-1/2}+1)(k_B\eta)^{1/2}(\Delta V)^{-5/6}{d_h}^2}{\rho(\nu Re)^{3/2}} \tag{36}$$

For the present work, we have performed five series of simulations, with the external parameter values fixed for each series. The values employed in each series of simulations are summarized in Table 1.

The first step of the numerical procedure is the choice of the volume $\mathrm{d}V$ and the corresponding dimensionless spatial grid step $\mathrm{d}x'$, and in our case $\mathrm{d}x' = \mathrm{d}V^{1/3}\,{d_h}^{-1}$. Next, the corresponding dimensionless time step $\mathrm{d}t'$ is evaluated from the CFL condition, $\mathrm{d}t' = Re(\mathrm{d}x')^2/6$. In selecting the number of temporal steps, the code needs to run, N_t, and we consider the temporal interval of $3\tau'_\sigma$ enough for the dying out of the transients due to the initial conditions. Hence, $N_t = 3\tau'_\sigma\,\mathrm{d}t'^{-1}$, where $\tau'_\sigma = C'^{-2}$. For instance, if $Re = 2$ and $\mathrm{d}V = 10^{-18}$ m^3, we have $\mathrm{d}x' = 0.0125$, $\mathrm{d}t' = 5.2094 \times 10^{-5}$, $C' = -10.27$, $\tau'_\sigma = 0.0095$, and $N_t = 546$.

Table 1. Simulations Parameters[a]

Re	$-\Pi_{0z}$	U_{CL} (m·s^{-1})	$-K$ ($10^5 \times$ N·m^{-3})
2	24	0.025	1.875
4	12	0.050	3.750
6	8	0.075	5.625
8	6	0.100	7.500
10	4.8	0.125	9.375

[a] $b = 50\,\mu$m, $c = 200\,\mu$m, $L = 800\,\mu$m, $d_h = 80\,\mu$m, $\rho = 10^3$ kg·m^{-3}, $\eta = 10^{-3}$ N·s·m^{-2}, $\mathrm{d}V = 10^{-18}$ m^3, $\mathrm{d}x = (\mathrm{d}V)^{1/3}$, $\Pi_{0x} = \Pi_{0y} = 10^{-2}\Pi_{0z}$, and a grid of 50 × 200 × 800 points.

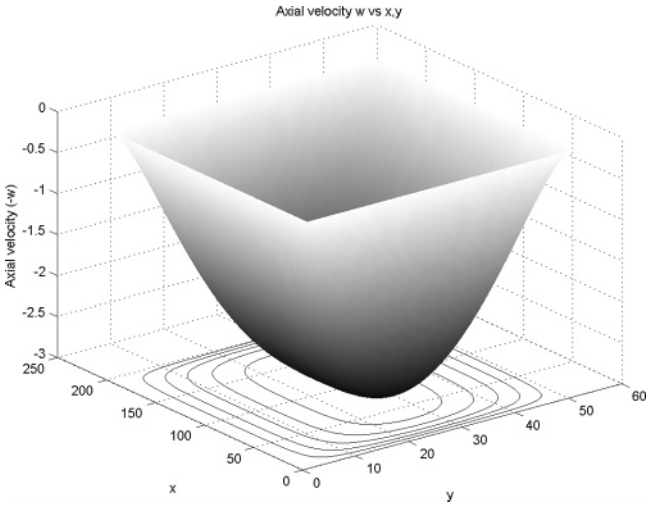

Figure 2. Dimentionless steady state solution for the component $w = w(x,y)$ of the velocity for $Re = 2$ (see Table 1 for other parameter values). The effect of the lateral pressure gradients $\partial_x p$ and $\partial_y p$ on the velocity profile is negligible.

To numerically evaluate the steady state solution, $[u^0_{i,j,k}, v^0_{i,j,k}, w^0_{i,j,k}]$, we proceed as follows: First, we initialize our working grid by setting all the matrix components of the velocities equal to zero, $[u_{i,j,k}, v_{i,j,k}, w_{i,j,k}] = 0$. We then fix the boundary conditions: $w(0,y,z) = w(b,y,z) = w(x,0,z) = w(x,c,z) = u(x,0,z) = u(x,c,z) = v(0,y,z) = v(b,y,z) = 0$. The values $u(0,y,z)$, $u(b,y,z)$, $v(x,0,z)$, $v(x,c,z)$, $w(x,y,0)$, and $w(x,y,L)$ are determined by the proper set of eq 35. Next, we solve simultaneously these three parts of eq 35. At every 10 time steps, we compute the difference between the actual velocities $[u_{i,j,k}, v_{i,j,k}, w_{i,j,k}]$ and the velocities in the previous verification. The maximum of the differences

$$\max([u^{t+10}_{i,j,k}, v^{t+10}_{i,j,k}, w^{t+10}_{i,j,k}] - [u^t_{i,j,k}, v^t_{i,j,k}, w^t_{i,j,k}])$$

is referred to as the error. Time integration of the equations is stopped when the error is less than the tolerance defined at the beginning of the process. We have found that a tolerance tol = 10^{-6} gives reasonable results for the steady state solution. In this first part of our numerical procedure (namely, the evaluation of the steady state solution) we use deterministic equations; that is, random noise is not considered. In all cases investigated, we obtained errors lower than the tolerance, indicating that the laminar solutions are stable, as expected from the very small Reynolds numbers employed in our calculations. An example of the steady state solution obtained by the above-described procedure is shown in Figures 2 and 3. In Figure 2 is shown the steady state solution for the axial component $w = w(x,y)$ of the velocity in a rectangular microchannel with $Re = 2$.

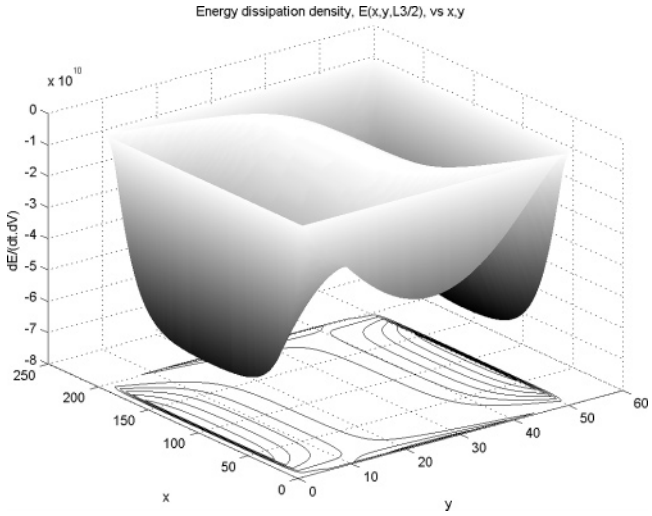

Figure 3. Energy dissipation per unit volume corresponding to the velocity profile shown in Figure 2. $Re = 2$, and other parameter values are quoted in Table 1. The asymmetry of the surface is because of the lateral pressure gradients $\partial_x p$ and $\partial_y p$.

In Figure 3 is displayed the energy dissipation per unit volume for the same microchannel of Figure 2. We note that the energy is mostly dissipated at the borders of the channel.

Once the steady state solution is evaluated, we start the second part of our simulations, aiming to compute fluctuations around the steady state solution due to thermal noise. Hence, we consider the complete set of eq 35 with the random term to the three evolution equations for the velocity components, solving the system over N_t temporal points and N_R realizations of the stochastic process. We obtain the perturbed three matrix $[u_{i,j,k},v_{i,j,k},w_{i,j,k}]$. To validate this procedure, we compared the average of the center line velocity with the deterministic one. The deviations were less than 0.01. We then analyzed the temporal and spatial correlations of the velocity fluctuations, focusing our study in the center line velocity w_{CL}.

IV. Results

A. Relaxation Time of Velocity Fluctuations. We display in Figure 4 the relaxation time τ_σ of the fluid velocity fluctuations as a function of the considered volume δV and the Reynolds number *Re*. We observe in Figure 4 that, for $\delta V = 1$ fl (10^{-18} m^3), τ_σ varies in the range 78 μs $\leq \tau_\sigma \leq$ 1.9 ms when *Re* varies in the range $2 \leq Re \leq 10$.

B. Autocorrelation Functions for the Central Line Velocity. We have performed a spectral analysis of the hydrodynamic fluctuations in the longitudinal component of the central line velocity. Our main result is that thermal noise excites the collective hydrodynamic modes at low frequencies (kHz). As an example of our results, we show in Figure 5a the normalized temporal autocorrelation function for the mean (over stochastic realizations) central line (CL) velocity for $Re = 2$. We observe that the correlation function extends up to 40 μs. Correspondingly, in Figure 5b, the Fourier transform of the former autocorrelation function (the spectral density of the CL velocity) goes up to the kHz region.

Regarding the spatial correlation, we show in Figure 6a the normalized spatial (*z* axis) autocorrelation function for the mean CL velocity. We can observe that the correlation is in the tenths of a millimeter range. Correspondingly, the Fourier transform of this function (Figure 6b) extends up to wavenumbers in the range of 10^3 m^{-1}. Our present results demonstrate the generic spatially long-range character of nonequilibrium fluctuations.

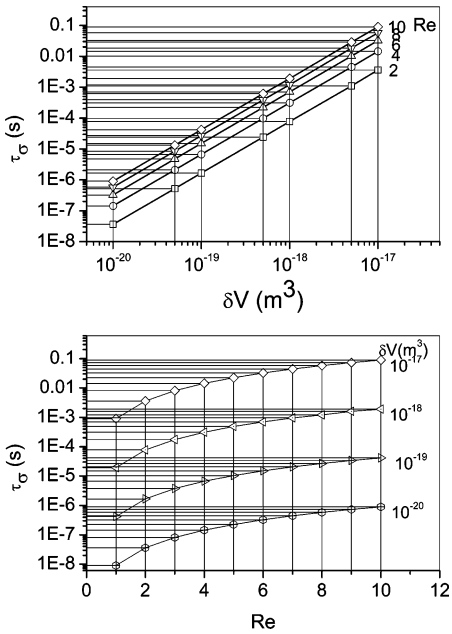

Figure 4. Relaxation time of the hydrodynamic fluctuations, τ_σ, as a function of the considered volume, δV, and the Reynolds number, *Re* (eqs 26 and 52).

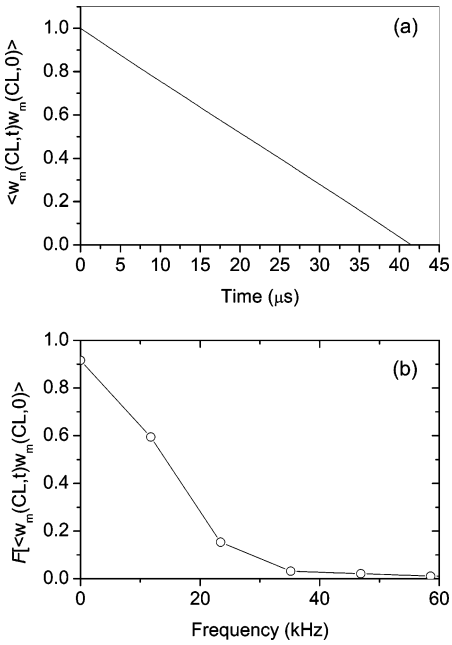

Figure 5. Normalized autocorrelation functions for $\langle w_{CL} \rangle$, $N_r = 200$, $N_t = 546$, and $Re = 2$: (a) temporal and (b) Fourier transform of the former temporal autocorrelation function (the spectral density).

This property was measured, indirectly, in light scattering experiments on fluids subject to a temperature gradient in which modifications to the Brillouin and Rayleigh lines were observed.[19,20] Also, such long-range correlations appear generically for a wide class of nonequilibrium states.[21] The predictions of this phenomenon have been made in a number of contexts,

(19) Beysens, D.; Garrabos, Y.; Zalczer, G. *Phys. Rev. Lett.* **1980**, *45*, 403−406; Wegdam, G. H.; Keulen, N. M.; Michielsen, J. C. F. *Phys. Rev. Lett.* **1985**, *55*, 630−633.

(20) (a) Law, B. M.; Sengers, J. V. *J. Stat. Phys.* **1989**, *57*, 531−547. (b) Law, B. M.; Segré, P. N.; Gammon, R. W.; Sengers, J. V. *Phys. Rev. A* **1990**, *41*, 816−824.

(21) (a) Dorfman, J. R.; Kirkpatrick, T.; Sengers, J. V. *Ann. Rev. Chem.* **1994**, *45*, 213. (b) Kirkpatrick, T.; Belitz, D.; Sengers, J. V. *J. Stat. Phys.* **2002**, *109* (3−4), 373−405.

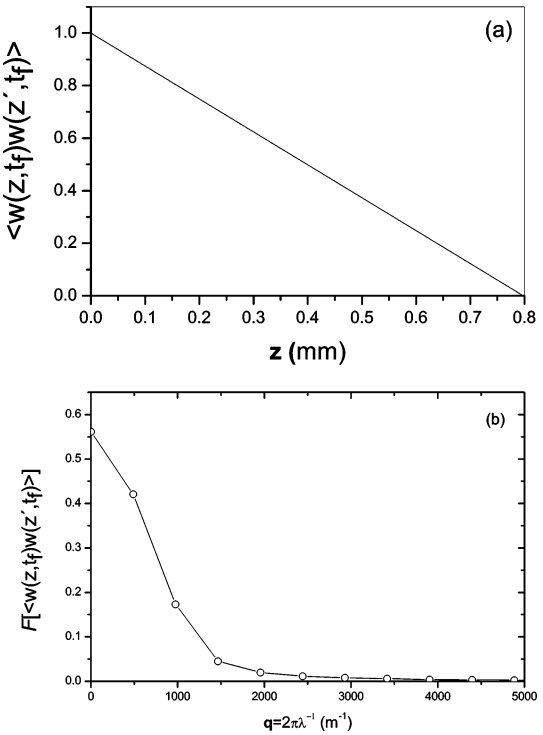

Figure 6. (a) Normalized spatial autocorrelation function (*z* axis), $Re = 2$. (b) Fourier transform of the former spatial autocorrelation function.

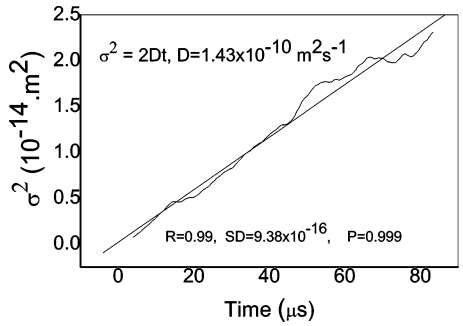

Figure 7. Variance, $\sigma^2 = \langle (z(t))^2 \rangle - \langle z(t) \rangle^2$, $Re = 2$, for the CL position in the long time limit as a funtion of time for $Re = 2$.

including self-organized criticality,[22] linear response,[23] nonequilibrium fluctuating hydrodynamics,[24,25] kinetic theory,[26] and stochastic hydrodynamics.[10,27,28,30]

C. Diffusion Coefficient. In Figure 7 is plotted the position variance along *z* in the long time limit as a funtion of time for $Re = 2$. From eq 18, we can obtain the effective diffusion coefficient of the fluid in the cell. We obtained the same value for the effective diffusion coefficient in the three directions $D_{\text{eff}} = 1.43 \times 10^{-10}\ \text{m}^2\cdot\text{s}^{-1}$, and as a consequence the fluid fluctuations could influence the diffusion of the probe molecule in some spectroscopies.

V. Conclusions

(1) By applying the Langevin dynamics, we have developed equations to computationally simulate the hydrodynamic fluctuations in a microchannel.

(2) We have determined the relaxation time of the hydrodynamic fluctuations in different volumes and Reynolds numbers (Figure 4).

(3) We have performed a spectral analysis of the hydrodynamic fluctuations for the CL velocity, for $Re = 2$, with the result that temporal correlations are in the microsecond range and that the thermal noise excites the hydrodynamic modes of low frequencies (kHz). Also, we observed long-range spatial correlation, and the wavenumber q (m^{-1}) is in the two digit range (Figures 5 and 6).

(4) We have determined the effective diffusion coefficient of the fluid in the cell for $Re = 2$, which is $D_{\text{eff}} = 1.43 \times 10^{-10}$ $\text{m}^2\cdot\text{s}^{-1}$, in the order of magnitude of the measurements reported in refs 12 and 13 for a similar system (Figure 7).

Acknowledgment. J.A.F. expresses his gratitude to Juan Pedro G. Villaluenga (Departamento de Física Aplicada I, Facultad de Ciencias Físicas, Universidad Complutense) for deep discussions while this work was done. We wish to thank the Fundación Santander-Central-Hispano (Programa de Visitantes Distinguidos UCM) for the support provided.

VI. Appendix: Fluctuation Correlations for the Random Stress Tensor

The correlations among the components of the random stress tensor are given by ref 16:

$$\langle s_{ik}(\mathbf{r},t) s_{lm}(\mathbf{r}',t') \rangle = 2k_{\text{B}}T\eta\left(\delta_{il}\delta_{km} + \delta_{im}\delta_{kl} - \frac{2}{3}\delta_{ik}\delta_{lm}\right)\delta(t-t')\,\delta(\mathbf{r}-\mathbf{r}') \quad (37)$$

In the case of $l = i$, $m = k$, in Cartesian coordinates

$$\langle s_{ik}(\mathbf{r},t) s_{ik}(\mathbf{r}',t') \rangle = A_{ik}\,\delta(t-t')\,\delta(x_1-x_1')\,\delta(x_2-x_2')\,\delta(x_3-x_3') \quad (38)$$

with A_{ik} given by

$$A_{ik} = 2k_{\text{B}}T\eta\left(1 + \frac{\delta_{ik}}{3}\right) \quad (39)$$

To perform simulations, we need to estimate the coefficient relating $(\partial s_{ik}(\mathbf{r},t)/\partial x_k)$ and the thermal noise. Deriving eq 38 with respect to x_k, we have

$$\frac{\partial \langle s_{ik}(\mathbf{r},t)\, s_{ik}(\mathbf{r}',t') \rangle}{\partial x_k} = \frac{A_{ik}}{x_k - x_k'}\delta(t-t')\,\delta(x_1-x_1')\,\delta(x_2-x_2')\,\delta(x_3-x_3') \quad (40)$$

For the δ function properties, including its derivative, consult the ref 31. Considering eqs 38 and 40 in the same volume ΔV and lapsus of time Δt, we obtain

$$\langle s_{ik}(\mathbf{r},t)^2 \rangle = A_{ik}(\Delta V)^{-1}(\Delta t)^{-1} \quad (41)$$

and

(22) Grinstein, G.; Lee, D. H.; Sachdev, S. *Phys. Rev. Lett.* **1990**, *64*, 1927.
(23) (a) Dufty, J. W. In *Spectral Line Shapes*; Wende, B., Ed.; W. de Gruyter: New York, 1981; p 1143. (b) *Long Range Correlations*; Buchler, J. R., Dufty, J. W., Kandrup, H. E., Eds.; Ann. NY Acad. Sci., Vol. 848; New York Academy of Sciences: New York, 1998; Vol. 848, p 1.
(24) Garcia, A. L.; Mansour, M. M.; Lie, G. C.; Mareschal, M.; Clementi, E. *Phys. Rev. A* **1987**, *36* (9), 4348−4355.
(25) Lutsko, J. F.; Dufty, J. W. *Phys. Rev. E* **2002**, *66*, 041206.
(26) Kirkpatrick, T. R.; Cohen, E. G. D.; Dorfman, J. R. *Phys. Rev. A* **1986**, *26*, 972.
(27) Schmitz, R. *Phys. Rep.* **1988**, *171*, 1−58.
(28) Ortiz de Zárate, J. M.; Sengers, J. V. *J. Stat. Phys.* **2004**, *115*, 1341−1359.
(29) Ortiz de Zárate, J. M.; Sengers, J. V. *Hydrodynamic Fluctuations in Fluids and Fluid Mixtures*; Elsevier: Amsterdam, 2006.
(30) Cattuto, C.; Brito, R.; Marconi, U. M. B.; Nori, F.; Soto, R. *Phys. Rev. Lett.* **2006**, *96*, 178001−178003.
(31) http//mathworld.wolfram.com/DeltaFunction.html, eq 14.

$$\frac{\partial\langle s_{ik}(\mathbf{r},t)^2\rangle}{\partial x_k} = -\frac{A_{ik}}{\Delta x_k}(\Delta V)^{-1}(\Delta t)^{-1} \tag{42}$$

or, deriving inside the bracket

$$\left\langle s_{ik}(\mathbf{r},t)\frac{\partial s_{ik}(\mathbf{r},t)}{\partial x_k}\right\rangle = -\frac{A_{ik}}{2\Delta x_k}(\Delta V)^{-1}(\Delta t)^{-1} \tag{43}$$

We perform now the following approximation inside the left bracket of the former equation:

$$s_{ik}(\mathbf{r},t) \sim \langle s_{ik}(\mathbf{r},t)^2\rangle^{1/2} \tag{44}$$

Finally, from eqs 40, 41, 43, and 44, we can write

$$\frac{\partial s_{ik}(\mathbf{r},t)}{\partial x_k} = -\frac{A_{ik}^{1/2}}{2\Delta x_k}(\Delta V)^{-1/2}\,\xi(t) \tag{45}$$

Replacing A_{ik} by its value given in eq 39, we have

$$\frac{\partial s_{ik}(\mathbf{r},t)}{\partial x_k} = \xi(t)\,C_i \tag{46}$$

with C_i given by

$$C_i = \sum_{k=1}^{3} B_{ik}$$

and B_{ik} given by

$$B_{ik} = -2^{-1/2}(k_B T\eta)^{1/2}\left(1+\frac{\delta_{ik}}{3}\right)^{1/2}(\Delta x_k)^{-1}(\Delta V)^{-1/2} \tag{47}$$

and

$$\overline{\frac{\partial s_{ik}(\mathbf{r},t)}{\partial x_k}} = \frac{1}{\Delta t}\int_t^{t+\Delta t}\frac{\partial s_{ik}(\mathbf{r},t)}{\partial x_k}\,dt = \frac{\sum_{k=1}^{3} B_{ik}}{\Delta t}\int_t^{t+\Delta t}\xi(t)\,dt = \frac{C_i}{\Delta t}\Delta W(t) \tag{48}$$

$\xi(t)$ is the thermal noise, defined by its statistical properties, namely

$$\langle\xi(t)\rangle = 0 \tag{49}$$

$$\langle\xi(t)\,\xi(t')\rangle = \delta(t-t') \tag{50}$$

that is, the correlation time of the noise is zero.

In eq 48, we use the definition of the Wiener's process (see refs 32 and 33), where $\Delta W(t)$ is the "Wiener's increment".

Considering $\Delta x_k = (\Delta V)^{1/3}$, then eq 47 for B_{ik} becomes

$$B_{ik} = -2^{-1/2}(k_B T\eta)^{1/2}(\Delta V)^{-5/6}\left(1+\frac{\delta_{ik}}{3}\right)^{1/2} \tag{51}$$

C_i then becomes independent of the index i, and we denote by C, namely

$$C = -2^{1/2}(3^{-1/2}+1)(k_B T\eta)^{1/2}(\Delta V)^{-5/6} \tag{52}$$

LA702502Q

(32) Gardiner, C. W. *Handbook of Stochastic Methods for Physics, Chemistry and the Natural Sciences*; Springer-Verlag: Berlin, 1985.

(33) Scherer, C. *Métodos Computacionais* da Física; Editora Livraria da Física, USP: São Paulo, 2005 (in Portuguese).